arXiv:1612.00146v1 [cond-mat.mes-hall] 1 Dec 2016

Conductance fluctuations in disordered 2D topological insulator wires: From quantum spin-Hall to ordinary quantum phases

Hsiu-Chuan Hsu,[1] Ioannis Kleftogiannis,[1] Guang-Yu Guo,[1,2] and Víctor A. Gopar[3]

[1] *Department of Physics, National Taiwan University, Taipei 10617, Taiwan*
[2] *Physics Division, National Center for Theoretical Sciences, Hsinchu 30013, Taiwan*
[3] *Departamento de Física Teórica and BIFI, Universidad de Zaragoza, Pedro Cerbuna 12, E-50009, Zaragoza, Spain*

(Dated: December 2, 2016)

Impurities and defects are ubiquitous in topological insulators (TIs) and thus understanding the effects of disorder on electronic transport is important. We calculate the conductance distributions of disordered 2D TI wires modeled by the Bernevig-Hughes-Zhang (BHZ) Hamiltonian with realistic parameters, and show that disorder drives the TIs into different quantum phases. We perform a statistical analysis of the conductance fluctuations in all quantum phases and find that although the BHZ Hamiltonian belongs to the symplectic symmetry class ($\beta = 4$), the conductance fluctuations follow the statistics of unitary universality class $\beta = 2$. Strong disorder, however, would drive the conductance fluctuations to universality class $\beta = 1$. At the phase transitions, the conductance distributions change drastically from one quantum phase to another due to the different degrees of localization of the helical edge and bulk states.

PACS numbers: 73.63.Nm, 71.70.Ej, 72.15.Rn, 73.43.Nq, 73.43.Jn

I. INTRODUCTION

Topological insulators (TIs) are currently at the forefront of fundamental research in condensed matter physics and their singular electronic properties, such as the existence of dissipationless helical edge states, make them potential candidates for practical uses in low power consumption and spin-based electronic devices [1]. Thus, an extensive literature covering fundamental and practical aspects of TIs already exists [2–5]. Most of the studies have been concentrated on pristine TIs, although the presence of disorder, such as impurities or lattice imperfections, is unavoidable in real devices.

The helical edge states of TIs are insensitive to weak disorder due to time-reversal (TR) symmetry, but strong disorder can still affect the electronic transport properties of TIs, as recently investigated [6–9]. For instance, the stability of the edge states in the presence of disorder has been studied in two-dimensional (2D) TIs and an unexpected quantum phase, the topological Anderson insulator, was discovered [6, 7]. Effects of disorder in three-dimensional TIs have been also investigated within the anomalous Aharonov-Bohm oscillations [10–13].

Disorder effects in low dimensional electronic devices have been a fundamental issue since early studies in the field of mesoscopic physics, particularly concerning the problem of quantum transport[14, 15]. It is known that multiple coherent scattering of electrons through disordered quantum wires can give a universal character to the transport in the sense that the statistical properties of the conductance fluctuations depend on few and general physical parameters of the system, such as TR and spin-rotation symmetries, whereas microscopic details are irrelevant. One known result on this respect is the constant value of the standard deviation of the conductance fluctuations in the diffusive regime, the so-called universal conductance fluctuations (UCF)[16], depending only on the presence of TR and spin-rotation symmetries: the UCF takes the value $\sqrt{8/15\beta}$, for $\beta = 1, 2$, and 4. The symmetry class $\beta = 1$ corresponds to systems that preserve both TR and spin-rotation symmetries, while $\beta = 2$ designates the cases with broken TR symmetry. If TR symmetry is preserved, but spin-rotation symmetry is broken, we have the symmetry class $\beta = 4$[15]. Therefore, a statistical study of the conductance fluctuations is naturally linked to the presence of disorder and symmetries play a fundamental role in the analysis.

Distribution moments of the conductance fluctuations such as the average and variance, have been recently experimentally and theoretically investigated in TIs [7, 17–21]. Although these two conductance moments provide important statistical information, they might not be sufficient for a full statistical description, especially when large conductance fluctuations are present, as frequently happens in experiments. A complete statistical description of the conductance fluctuations is provided by the full distribution of the conductance. To the best of our knowledge, few works have been devoted to the study of the distribution of the conductance fluctuations in TIs[22, 23]. In Ref. [22], the conductance fluctuation in a quantum network model is analyzed via the distribution of transmission eigenvalues, while in Ref. [23] a Bernevig-Hughes-Zhang (BHZ) tight-binding model has been considered to study numerically the conductance distribution in topological Anderson insulators. Thus, a thorough theoretical analysis of the conductance fluctuation in 2D TI is needed.

In this work, we first calculate the conductance distributions of disordered 2D TI wires modeled by a BHZ Hamiltonian describing an inverted InAs/GaSb quantum

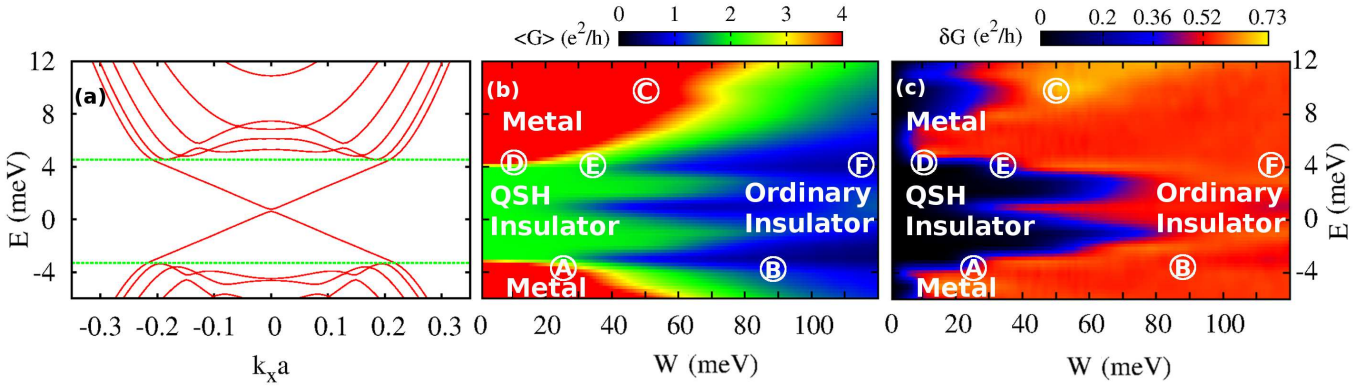

FIG. 1. (Color online) (a)The band structure of an InAs/GaSb nanowire with $N = 60$. The green dashed lines indicate the energy range where helical edge states occur. The phase diagrams of (b) the mean conductance $\langle G\rangle$ and (c) the standard deviation δG in the $E - W$ plane using 5000 disorder configurations. Circled letters denote the points where conductance distributions are calculated, as shown in Figs. 2-4.

well known for its practical advantages over other 2D TI materials, including the well-developed material control for fabrication and the tunable band structure by electric fields [24, 25]. We obtain the phase diagrams of the mean and standard deviation of the conductance, which reveal three different quantum phases: the metallic (M), the ordinary insulating (OI), and the quantum spin Hall insulating (QSHI) phase. Secondly, to get a full understanding of the statistical properties in each phase and at the transitions, we perform a theoretical analysis based on random matrix theory(RMT)[26]. We find that the conductance distributions for 2D TI wires follow the $\beta = 2$ symmetry class in all the phases and transitions except in the strongly disordered metallic region, despite the fact that the BHZ Hamiltonian is TR invariant. At the M-QSHI transition, we need to take into account the different extents of localization of the conducting channels to describe the asymmetric distribution centered around the average conductance $\langle G\rangle = 2$. For simplicity, the unit of the conductance of e^2/h is omitted throughout this paper. Similarly, as the system is driven from the QSHI to the OI phase, the conductance deviates significantly from $G = 2$, although its fluctuation can be described as in the OI phase ($\beta = 2$). Our analysis reveals that the edge states play an important role at the phase transitions that involve the QSHI phase and the symmetry of the Hamiltonian alone is not enough to obtain a full understanding of the statistical properties of the conductance at these transitions.

II. THEORY AND METHODS

We adopt the BHZ model in the tight-binding representation to describe the electronic properties of the clean InAs/GaSb TI wires [6, 25, 27]. The Hamiltonian H consists of two terms: $H = H_c + H_d$, where H_c corresponds to a clean (disorder free) TI wire, and H_d contains a source of disorder. The H_c term can be written in a block diagonal form as

$$
\begin{aligned}
H_c &= \sum_{ip} V c_{ip}^\dagger c_{ip} + t_{xp} c_{ip}^\dagger c_{i+\delta x,p} + t_y c_{ip}^\dagger c_{i+\delta y,p} + h.c. \\
V &= \begin{pmatrix} -4D + M - 4B & 0 \\ 0 & -4D - M + 4B \end{pmatrix} \\
t_{xp} &= \begin{pmatrix} D + B & -iAp/2 \\ -iAp/2 & D - B \end{pmatrix} \\
t_y &= \begin{pmatrix} D + B & A/2 \\ -A/2 & D - B \end{pmatrix},
\end{aligned} \tag{1}
$$

where $p = \pm$ denotes the pseudospin, $i = (x, y)$ is the site index and $\delta x(y)$ is the vector to the nearest neighbor along the $x(y)$-direction. The matrices V, t_{xp}, t_y are in the basis of electron and hole states. The parameters A, B, D, M are material-dependent. We use the values for those parameters of a InAs/GaSb quantum well derived from $k\cdot p$ method [25, 27]: $A = 18.5$ meV, $B = -165$ meV, $D = -14.5$ meV, $M = -7.8$ meV with the lattice constant $a = 2$ nm. The Hamiltonian preserves time-reversal symmetry that prevents backscattering of the edge states. For simplicity, we neglect the bulk and structure inversion asymmetry which do not affect the topology of the Hamiltonian.

A source of disorder is introduced in the Hamiltonian model by considering a random on-site energy as

$$
H_d = \sum_{ip} \epsilon_i c_{ip}^\dagger I c_{ip} \tag{2}
$$

where ϵ_i is a random number uniformly distributed in the range $[-W/2, W/2]$ and I is the 2×2 identity matrix.

The above BHZ tight-binding Hamiltonian model is solved numerically. The conductance G is calculated by

attaching a perfect lead to each side of the InAs/GaSb wire. Within the Landauer-Büttiker formalism [28] the conductance is given by $G = \frac{2e^2}{h}\sum_i^n \tau_i$, where τ_i are the transmission eigenvalues of $tt^\dagger$, t being the $n \times n$ transmission matrix with $n = 2N$, where N is the width of the wire in units of the lattice constant.

III. RESULTS AND DISCUSSION

A. Phase Diagrams

The calculated band structure of a pristine InAs/GaSb wire is shown in Fig. 1(a). Unless stated otherwise, we set the number of sites along the y- and x-direction to $N = 60$ and $L = 300$, respectively, and assume the transport to be along the x-direction. The edge states occur in the energy window $[-3.36, 4.55]$ meV. The presence of disorder, however, changes the quantum phase of TIs and some signatures of these phases can be seen in the phase diagram of the ensemble average conductance $\langle G\rangle$ in the energy-disorder strength $(E-W)$ plane [see Fig. 1 (b)]. From this phase diagram, we can identify the QSHI phase characterized by a constant average $\langle G\rangle = 2$, in the energy range of $[-3.36, 4.55]$ meV (green area) and up to a disorder strength $W = 40$ meV, approximately. If the energy is increased, within the same range of disorder strength, the TI wire changes to the metallic phase, whereas if the strength of disorder is increased within the energy window $[-3.36, 4.55]$meV, the TI wire becomes an ordinary insulator.

Further useful information can be obtained by plotting the standard deviation of the conductance $\delta G = \sqrt{(G - \langle G\rangle)^2}$ in the E–W plane. From the δG phase diagram shown in Fig. 1 (c), we observe that for energies in $[-3.36, 4.55]$ meV and until disorder strength $W = 40$ meV (black region) the conductance fluctuations are negligible, revealing the robustness of the edge states against disorder in the QSHI regime. For higher energies, however, the standard deviation takes the UCF value $\delta G = \sqrt{4/15} \approx 0.52$, which is the representative value of the metallic phase for $\beta = 2$. We notice also that at strong disorder strength and high energy, δG reaches the value 0.73 (yellow region in Fig. 1 (c)), which corresponds to the UCF for the symmetry class $\beta = 1$. Next we perform a statistical analysis of the conductance distribution in each phase.

B. Metal - Ordinary Insulator Transition

We first study the evolution of the conductance distribution from the M to the OI phase as the strength of disorder increases. In Fig. 2 (a), we show $P(G)$ for three different values of the W at fixed energy $E = -4$ meV. In all the distributions shown below, the histograms are

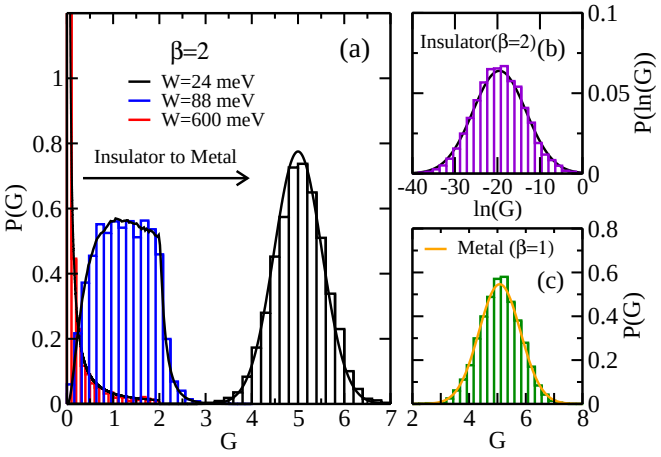

FIG. 2. (Color online) (a)Conductance distributions at $E = -4$ meV for different disorder strengths W showing the transition from M to OI phase. $W = 24/88$ meV corresponds to the point Ⓐ/Ⓑ in the phase diagrams in Fig. 1. The mean conductance $\langle G\rangle = 5, 1.2, 0.07$ for $W = 24, 88$ and 600 meV, respectively. (b) The log-normal distribution for the OI phase at $E = -4, W = 1000$ meV ($\langle G\rangle = 5 \times 10^{-4}, \langle \ln(G)\rangle = -19.5$). (c) Conductance distribution of the point Ⓒ in the phase diagrams in Fig. 1. The behavior for the $\beta = 1$ universality class is recovered resulting in a Gaussian distribution with $\delta G = 0.73$ centered at 5.1. (orange fitting curve).

obtained by numerical calculation using 10000 disorder realizations. In the M regime, when $W = 24$ meV, the conductance distribution follows the expected Gaussian distribution (solid line). The variance of the Gaussian distribution is given by the UCF: $\sqrt{4/15}$ ($\beta = 2$), i.e., $P(G)$ is given by:

$$P(G) = \sqrt{\frac{15}{8\pi}} e^{-\frac{15}{8}(G-\langle G\rangle)^2} \tag{3}$$

with $\langle G\rangle = 5$ for the case shown in Fig. 2 (a).

Interestingly, we note that the value of the UCF ($\sqrt{4/15}$) corresponds to the physical systems with broken TR symmetry, i.e., $\beta = 2$ universality class. The BHZ Hamiltonian, however, preserves TR symmetry. Moreover, due to the spin-orbit coupling (SOC) term, one would expect that the UCF follows that of the symplectic class ($\beta = 4$). This apparently contradictory finds its origin in the block diagonal structure of the Hamiltonian (see Eq. (1)): each block breaks TR symmetry and belongs to the $\beta = 2$ symmetry, i.e., the conductance G is given by the identical contribution of the two Hamiltonian blocks with $\beta = 2$ symmetry class.

As the strength of disorder is increased, the Gaussian distribution becomes wider and the Gaussian landscape is lost. In Fig. 2 (a) we show an example ($W = 88$ meV) of $P(G)$ in the crossover between the M and OI regime (blue histogram). In this case, the conductance fluctuations are large. In particular, for the case shown in Fig. 2

(a), the relative fluctuations $\delta G/\langle G\rangle$ are five times larger than in the previous metallic phase (black histogram). The theoretical curve (solid line) that describes the numerical simulations (blue histogram) has been obtained from the joint distribution $P_s(\{\tau_i\})$ $(i = 1, 2, \ldots, n)$ of the different transmission eigenvalues τ_i, or channels, together with the Landauer-Büttiker expression for the conductance. Within the Dorokhov-Mello-Pereyra-Kumar approach of the RMT [26], the joint distribution $P(\{\tau_i\})$, where τ_i are the eigenvalues of the transmission matrix, follows a diffusion equation which describes the evolution of $P(\{\tau_i\})$ with the length of the disordered system. For the unitary symmetry class $\beta = 2$, $P(\{\tau_i\})$ is conveniently written in terms of the variables $x_i = \mathrm{acosh}[1/\sqrt{\tau_i}]$ as [30],

$$p(\{x_i\}) = \frac{1}{Z}\exp\left[-H(\{x_i\})\right], \tag{4}$$

where $Z = \int \Pi_i dx_i \exp[-H(\{x_i\})]$ and $H(x_i) = \sum_{i<j}^{n} u(x_i, x_j) + \sum_i^n V(x_i)$.

In both the metallic and ordinary insulating regimes, the functions $u(x_i, x_j)$ and $V(x_i)$ can be written as [30, 31]:

$$\begin{aligned} u(x_i, x_j) &= \ln\left|\sinh^2 x_i - \sinh^2 x_j\right| + \ln\left|x_i^2 - x_j^2\right|, \\ V(x_i) &= ns^{-1}x_i^2 - \frac{1}{2}\ln\left|x_i \sinh 2x_i\right|, \end{aligned} \tag{5}$$

where $s = L/nl$, l being the mean free path and n the number of conducting channels.We point out that the ratio s is the only microscopic information that plays a role in the above model and can be determined by the mean conductance $\langle G\rangle$. For instance, in the metallic limit, $\langle G\rangle = \xi/L$, where ξ is the localization length and equals to nl , while in the ordinary insulating limit, $\langle G\rangle = e^{-\xi/L}$. In our analysis, s is tuned in the integration till the resultant $\langle G\rangle$ reaches the numerical value.

Using the joint distribution $P(\{\tau_i\})$ (or equivalently $p(\{x_i\})$) we calculate the conductance distribution given by

$$P(G) = \left\langle \delta(G - 2\sum_i^n \tau_i)\right\rangle, \tag{6}$$

where the brackets represent the average performed with the probability density function $p(\{x_i\})$, Eq. (4). Thus, $P(G)$ can be calculated by numerical integration.

For the present case, the theoretical distribution (solid line) $P(G)$ is obtained using the first two channels ($n = 2$), since the conductance values are not larger than 4, indicating that no more than two different channels from each block Hamiltonian contribute to the conductance, while with the ratio $L/l = 5.2$ is found to reproduce the numerical average conductance $\langle G\rangle = 1.2$. Fig. 2 (a) shows a good agreement between the theoretical (solid line) and numerical (blue histogram) distributions.

Let us now increase further the strength of disorder to $W = 600$ meV. In the presence of strong disorder, the main contribution to the conductance comes from a single transmission eigenvalue and therefore the multivariate distribution $P(\{\tau_i\})$ is simplified to the distribution of a single variable, $P(\tau)$. In this case, we can write an analytical expression for the probability density of the conductance $P(G)$ as [29]:

$$P(G) = C\frac{\mathrm{acosh}^{1/2}(\sqrt{2/\mathrm{G}})}{G^{3/2}(2-G)^{1/4}}\exp\left[(-l/L)\mathrm{acosh}^2\left(\sqrt{2/G}\right)\right], \tag{7}$$

where C is a normalization constant. As in the previous multichannel case, the ratio $s = L/l$ plays an important role since all the statistical properties of the conductance fluctuations are fixed by this ratio. For one channel, L/l can be extracted from the numerical simulations using $L/l = \langle -\ln(G/2)\rangle$. In Fig. 2(a), the conductance distribution (solid line) for $W = 600$ meV according to Eq. (7) is plotted. A good agreement between theory (solid line) and the numerical simulations (red histogram) is seen.

If we increase even further the strength of the disorder, the TIs reach the deeply insulating limit and the conductance distribution follows a log-normal distribution [30, 31], as shown for $W = 1000$ meV in Fig. 2 (b). The numerical distribution (histogram) for $\ln G$ is well described by $P(\ln G) = 1/\sqrt{2\pi\sigma^2}\exp\left[-(\ln G - \langle \ln G\rangle)^2/2\sigma^2\right]$ with $\sigma^2 = 2\langle -\ln G\rangle$. The value of $\langle \ln G\rangle$ has been obtained from the numerical calculations.

Finally, we note that in Fig. 1 (c) for high energy ($E > 8$ meV) and the disorder strength of $\sim$50 meV, δG can reaches $\sqrt{8/15} \approx 0.73$ (yellow region), which corresponds to the UCF for the orthogonal symmetry ($\beta = 1$), i.e., the symmetry class for systems with TR symmetry and no SOC. This reveals that the contribution from SOC is negligible in comparison with the effects of the disorder, which are introduced through a TR symmetric term in the Hamiltonian model as given in Eq. 2. A similar behavior of the crossover between symmetry classes $\beta = 1$ and $\beta = 4$ has been reported in [32]. Since disorder alone belongs to the symmetry class $\beta = 1$, the conductance fluctuations follow a Gaussian distribution with variance $\sqrt{8/15}$, as shown in Fig. 2(c).

C. Metal - Quantum spin Hall Transition

In the M phase the conductance fluctuations follow a Gaussian distribution, as shown above. On the contrary, in the QSHI phase, there is no conductance fluctuation due to the robustness of the helical edge states against disorder. Thus, it is of interest to study the conductance fluctuations at the transition between these two phases, when both edge and bulk states contribute to the conductance.

In our numerical simulations, we have chosen the point

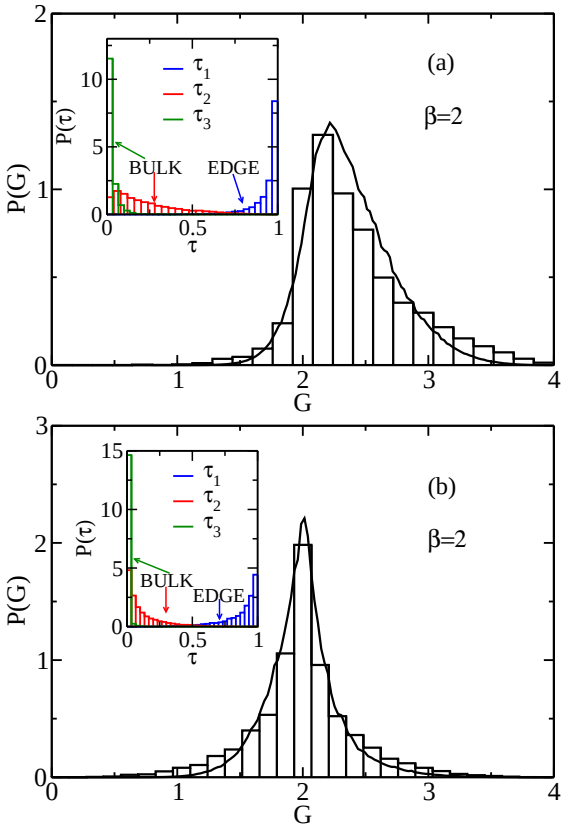

FIG. 3. (Color online) The conductance distribution with $\langle G\rangle = 2.39$ at the M-QSHI transition at $E = 4.55$ meV and $W = 12$ meV for two different system lengths (a) L=300, corresponding to Ⓓ in the phase diagrams in Fig. 1 and (b) L=600. The solid line is the theoretical distribution. The probability distributions of the three largest transmission eigenvalues τ_1, τ_2, τ_3 are shown in the inset.

at the phase transition: $W = 12, E = 4.55$ meV (point Ⓓ in Fig. 1(b) and (c)). At this M-QSHI transition point, we have analyzed the fluctuations of the first three largest different eigenvalues, represented by τ_1, τ_2 and τ_3. These three channels give the main contribution to total conductance G. In the inset of Fig. 3(a) and (b), we show the distribution of each transmission eigenvalue for two different TI wire lengths ($L = 300$ and 600, respectively). The first transmission eigenvalue τ_1 is associated to the helical edge state which is highly transmitted, whereas the second and third transmission eigenvalues are associated to the bulk states which are poorly transmitted. Hence, the distribution of the first eigenvalue peaks at $\tau_1 = 1$, while the distribution of τ_2 and τ_3, respectively, peaks at zero. This suggests that helical edge states are weakly localized, whereas bulk states are strongly localized. Therefore, in order to describe the conductance fluctuations, we need to introduce the information about the different strengths of localization of the edge and bulk states.

We note that the information about the electron localization in our model is given by parameter $s = L/l$ (see Eqs. 5 and 7), determined by $\langle \ln G\rangle$ in the case of one transmission channel. Therefore, in order to study different localizations, we introduce a different s_i value for each transmission eigenvalue, determined by the numerical calculations. For the case shown in Fig. 3 we found that $\langle -\ln \tau_2\rangle$ is 25 times larger than $\langle -\ln \tau_1\rangle$, while $\langle -\ln \tau_3\rangle$ is 60 times larger than $\langle -\ln \tau_1\rangle$. Thus, we set $s_2 = 25 s_1$ and $s_3 = 60 s_1$ with $s_1 = 0.34$ fixed to reproduce the average conductance $\langle \ln G\rangle$, or equivalently $\langle G\rangle$. In Fig. 3, we show the distribution $P(G)$ obtained in this way. In 3(b) we show another example of a longer TI wire where the trend of the distributions is also well described by our model. Distributions with similar characteristics at the M-QSHI transition of a Z2 network model were reported in [22], which, however, were derived numerically for the symplectic class ($\beta = 4$), whereas our case is for the unitary class $\beta = 2$. We find that the asymmetric property of the distribution at the M-QSHI transition is not determined by the symmetry class, but rather, by the different localizations of the different conducting channels.

D. Ordinary Insulator - Quantum Spin Hall Transition

As shown above, helical edge states are robust against disorder. However, at strong disorder strength, edge states become localized eventually, leading the QSHI phase to an OI phase. At this transition, but on the QSHI side , the conductance distribution has a large peak at $G = 2$, as shown in Fig. 4 (a), because the edge states have not yet been fully localized. In contrast, on the OI side, the distribution shows a peak at $G = 0$ [Fig. 4 (b)], indicating that the edge states become localized.

To study the fluctuations on the QSHI side, we consider that the presence of the edge states only shifts the value of the average conductance to 2, but the conductance fluctuations come from the localized edge states penetrating into the bulk, whose conductance distribution can be described by Eq. (7) as in the OI phase. We thus only need to make the change of variable $G \to 2-G$ in Eq. (7) to obtain the conductance distribution.

$$P(G) = C\frac{\sqrt{\mathrm{acosh}\sqrt{\frac{2}{2-G}}}}{(2-G)^{3/2}G^{1/4}}\exp\left[-s'^{-1}\mathrm{acosh}^2\sqrt{\frac{2}{(2-G)}}\right], \quad (8)$$

where C is a normalization constant and s' is determined by the average $s' = \langle \ln(2-G)/2\rangle$. Fig. 4 (a) shows a theoretical $P(G)$ (solid line) which agrees well with numerical simulations (histograms). Regarding the OI to QSHI transition, but on the OI side, the perfect conducting edge states become localized and the TI becomes

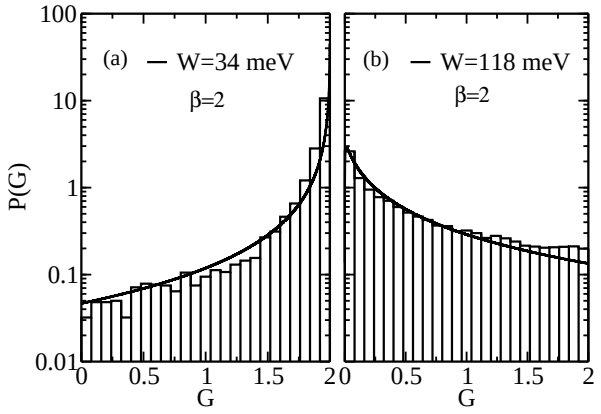

FIG. 4. Conductance distributions at the QSHI-OI phase transition at $E = 4$, $W = 34$ meV (a) and $W = 118$ meV (b) corresponding to the points Ⓔ and Ⓕ in the phase diagram in Fig. 1. Solid lines are theoretical distributions.

an ordinary insulator. Only a single transmission eigenvalue is relevant and the distribution of conductances is described by Eq. (7). Fig. 4 (b) shows both the numerical (histogram) and theoretical (solid line) distribution for $P(G)$.

IV. CONCLUSIONS

TIs are not free of impurities and/or lattice defects and therefore a full understanding of the effects of the disorder on the electronic transport is important. We have calculated the conductance distributions of disordered 2D TI wires modeled by a BHZ Hamiltonian with experimentally achievable parameters, and have obtained the phase diagrams of the mean and the deviation of the conductance, which reveal three different quantum phases. We have also carried out a statistical analysis of the conductance fluctuations produced by the presence of disorder in all quantum phases of 2D TI wires.

Interestingly, we find that although TR symmetry is preserved and spin rotation symmetry is broken in the BHZ Hamiltonian, which corresponds to the symplectic symmetry $\beta = 4$, the conductance fluctuations follow the statistics of the unitary class $\beta = 2$. This is a consequence of the block diagonal structure of the Hamiltonian in which each block belongs to the unitary class $\beta = 2$. At strong disorder, however, the effects of the SOC are negligible and the conductance fluctuations follow the statistics of the universality class $\beta = 1$. Furthermore, our results reveal that at M-QSHI and OI-QSHI phase transitions, both bulk and helical edge states contribute to the conductance, albeit with different extent of localization. Consequently, the conductance distributions change drastically from one quantum phase to another due to the different degree of localization of the helical edge and bulk states as well as the number of relevant transmission channels. We thus believe that the extensive analysis of the conductance fluctuations presented here gives a complete picture of the statistics of the conductance fluctuations and offers deeper insights into the quantum transport in disordered TIs.

ACKNOWLEDGEMENTS

H.-C. H. would like to thank Dong-Hui Xu for helpful discussions. V. A. G acknowledges support from MINECO (Spain) under the Project number FIS2015-65078-C2-2-P and hospitality of Physics Department and Center for Theoretical Sciences of the National Taiwan University. H.-C. H., I. K. and G.-Y. G. acknowledges support from Academia Sinica, National Center for Theoretical Sciences and the Ministry of Science and Technology of The R.O.C. The authors gratefully acknowledge the resources from the supercomputer "Terminus", technical expertise and assistance provided by the Institute for Biocomputation and Physics of Complex Systems (BIFI) - Universidad de Zaragoza" as well as from the National Center of High-performance Computing of Taiwan.

REFERENCES

[1] X.-L. Qi and S.-C. Zhang, Rev. Mod. Phys. **83**, 1057 (2011).
[2] C. L. Kane and E. J. Mele, Phys. Rev. Lett. **95**, 226801 (2005).
[3] M. Z. Hasan and C. L. Kane, Rev. Mod. Phys. **82**, 3045 (2010).
[4] T.-W. Chen, Z.-R. Xiao, D.-W. Chiou, and G.-Y. Guo, Phys. Rev. B **84**, 165453 (2011).
[5] B. A. Bernevig, T. L. Hughes, and S. C. Zhang, Science, **314**, 1757 (2006).
[6] H. Jiang, L. Wang, Q.-f. Sun, and X. C. Xie, Phys. Rev. B **80**, 165316 (2009).
[7] J. Li, R.-L. Chu, J.K. Jain and S.-Q. Shen, Phys. Rev. Lett. **102**, 136806 (2009).
[8] K.-I. Imura, Y. Kuramoto, and K. Nomura, Phys. Rev. B **80**, 085119 (2009).
[9] C.-Z. Chen, H. Liu, H. Jiang, Q.-F. Sun, Z. Wang, and X. C. Xie, Phys. Rev. B **91**, 214202 (2015).
[10] Y. Zhang and A. Vishwanath, Phys. Rev. Lett. **105**, 206601(2010).
[11] J. H. Bardarson, P. W. Brouwer, and J. E. Moore, Phys. Rev. Lett. **105**, 156803 (2010).
[12] S. Cho, B. Dellabetta, R. Zhong, J. Schneeloch, T. Liu, G. Gu, M. J. Gilbert, and N. Mason, Nat. Commun. **6**, 8634 (2015).
[13] R. Du, H.-C. Hsu, A. C. Balram, Y. Yin, S. Dong, W. Dai, W. Zhao, D. S. Kim, S.-Y. Yu, J. Wang, X. Li, S. E.

Mohney, S. Tadigadapa, N. Samarth, M. H. W. Chan, J. K. Jain, C.-X. Liu, and Q. Li, Phys. Rev. B **93**, 195402 (2016)
[14] Y. Imry, *Introduction to Mesoscopic Physics* (Oxford University Press, Oxford, 1997).
[15] C. Beenakker, Rev. Mod. Phys. **69**, 731 (1997)
[16] P. A. Lee and A. D. Stone, Phys. Rev. Lett. **55**, 1622 (1985)
[17] S. Matsuo, K. Chida, D. Chiba, T. Ono, K. Slevin, K. Kobayashi, T. Ohtsuki, C.-Z. Chang, K. He, X.-C. Ma and Q.-K. Xue, Phys. Rev. B **88**, 155438(2013).
[18] A. Kandala, A. Richardella, D. Zhang, T. C. Flanagan, and N. Samarth, Nano Lett. **13(6)**, 2471 (2013).
[19] Z. Li, Y. Meng, J. Pan, T. Chen, X. Hong, S. Li, X. Wang, F. Song and B. Wang, Appl. Phys. Express, **7**, 065202 (2014).
[20] Y. Takagaki, Phys. Rev. B **85**, 155308 (2012).
[21] D.-H. Choe, and K. J. Chang, Sci. Rep. 5, 10997 (2015).
[22] K. Kobayashi, T. Ohtsuki, H. Obuse, and K. Slevin, Phys. Rev. B **82**, 165301 (2010).
[23] D. Xu, J. Qi, J. Liu, V. Sacksteder, X. C. Xie, and H. Jiang, Phys. Rev. B **85**, 195140 2012.
[24] I. Knez, and R. Du, Front. Phys. **7**, 200 (2012).
[25] C. X. Liu, T. L. Hughes, X.-L. Qi, K. Wang, and S. C. Zhang, Phys. Rev. Lett. **100**, 236601 (2008).
[26] P. A. Mello and N. Kumar, *Quantum Transport in Mesoscopic Systems: Complexity and Statistical Fluctuations* (Oxford University Press, Oxford, 2004).
[27] D.-H. Xu, J.-H. Gao, C.-X. Liu, J.-H. Sun, F.-C. Zhang, and Y. Zhou, Phys. Rev. B **89**, 195104 (2014).
[28] S. Datta, *Electronic transport in mesoscopic systems* (Cambridge University Press, Cambridge, England, 1995).
[29] V. A. Gopar and R. A. Molina, Phys. Rev. B **81**, 195415 (2010).
[30] C. W. J. Beenakker, and B. Rejaei, Phys. Rev. Lett. **71**, 3689 (1993).
[31] K. A. Muttalib, P. Wölfle, V. A. Gopar, Annals of Physics **308**, 156 (2003).
[32] T. Kaneko, M. Koshino and T. Ando, Phys. Rev. B **81**, 155310 (2010).